Princeton Plasma Physics Laboratory

PPPL-5235

Resonance in Fast-Wave Amplitude in a Low-Density Peripheral Plasma

R. J. Perkins and J. C. Hosea and N. Bertelli and G. Taylor and J. R. Wilson

January 2016

Prepared for the U.S. Department of Energy under Contract DE-AC02-09CH11466.

Princeton Plasma Physics Laboratory
Report Disclaimers

Full Legal Disclaimer

Trademark Disclaimer

PPPL Report Availability

Princeton Plasma Physics Laboratory:

http://www.pppl.gov/techreports.cfm

Office of Scientific and Technical Information (OSTI):

http://www.osti.gov/scitech/

Related Links:

U.S. Department of Energy

U.S. Department of Energy Office of Science

U.S. Department of Energy Office of Fusion Energy Sciences

Resonance in Fast-Wave Amplitude in a Low-Density Peripheral Plasma

R. J. Perkins and J. C. Hosea and N. Bertelli and G. Taylor and J. R. Wilson
Princeton Plasma Physics Laboratory, Princeton, NJ 08540

Wave propagation across inhomogeneous plasma is a critical issue for high-power plasma heating systems using waves in the ion cyclotron frequency range. Efficient coupling across the low-density scrape-off layer (SOL) has been especially challenging on the National Spherical Torus eXperiment (NSTX), where a large fraction of the wave power is lost to the divertor along SOL field lines. Using a cylindrical cold-plasma model, we demonstrate a special class of modes that carries a large fraction of the wave energy along the peripheral plasma. The modes occur when the radial fast-wave phase difference across the SOL is roughly $\pi/2$, leading to a pronounced increase in wave amplitude. Such modes could be important in explaining the loss of fast-wave power on NSTX. They also demonstrate how a small layer of diffuse plasma can drastically alter the global wave solution.

Wave propagation across inhomogenous plasma is a broad topic of importance to the magnetosphere [1], the solar corona [2], and the ionosphere [3]. It is crucial for magnetically confined fusion experiments that employ multi-megawatt heating systems based on waves in the ion cyclotron range of frequencies (ICRF). Such systems are a leading candidate for heating burning plasmas due to proven wave physics in the core plasma and readily available high-power sources in this frequency range. However, the key challenge is coupling waves across a steep density gradient: the density rises from below 10^{17} m^{-3} at the launching antenna near the outer edge to intermediate values of the order of 10^{18} m^{-3} in the scrape-off layer (SOL), and then to values of order 10^{19} m^{-3} as one enters the core. ICRF waves typically transition from being radially cutoff at the antenna to fully propagating somewhere in the SOL. This transition is critical in high-harmonic fast-wave (HHFW) heating on the National Spherical Torus eXperiment (NSTX), where up to 60% of the coupled HHFW power is hypothesized to be lost to waves propagating in the SOL but never penetrating the core [4]. Full-wave simulations of NSTX using the AORSA code [5], with the solution domain extended to include the SOL [6], show that the RF electric field grows large in the SOL when the density at the antenna exceeds the right-hand cutoff density [6, 7]. However, interpretation of the AORSA results is complicated by vessel and magnetic geometry [8], and the fundamental reason for these losses was not fully understood. This limits our ability to mitigate the losses, which limits the operational scenarios available to the NSTX program. It also limits predictive capability regarding the potential impact of such losses on future fusion experiments, such as the multi-billion dollar ITER project [9].

We use a cylindrical cold-plasma model to demonstrate a special type of mode that conducts significant wave power in the low-density peripheral plasma. We refer to these modes as annulus resonances due to their enhanced amplitude and unique radial distribution of wave power. This is a resonance of a radially bounded system, not to be confused with the unbounded wave resonance condition $k \to \infty$. Annulus resonances occur when the phase difference across the SOL approaches $\pi/2$ and demonstrate how a small region of diffuse plasma can drastically alter the global solution; similar modes might conceivably arise in applications outside of fusion. These resonances are strong candidates for explaining the SOL losses observed on NSTX and for explaining why AORSA computes large amplitude RF fields in the SOL in some scenarios but not others. The model is based upon that in Refs. [10–12], where similar results regarding edge wave propagation were found for ion cyclotron waves (slow waves) below the ion cyclotron frequency [12]. The present results are for fast waves above the ion cyclotron frequency. The cylindrical model is computationally inexpensive and allows a detailed study of individual modes, which is important for the identification of the annulus resonances. Understanding these modes may help minimize SOL losses on NSTX-U, as indicated below, and guide work with full-wave codes to predict ICRF coupling on burning plasma devices such as ITER.

The model geometry, shown in Fig. 1, consists of three radial regions: a core plasma, a lower-density annulus, and an outer vacuum region. The core extends to radius r_c with constant density n_c. The annulus extends from $r = r_c$ to r_a with constant density n_a. The vacuum region extends from $r = r_a$ up to a conducting wall of radius r_w. A uniform axial magnetic field is used throughout. The antenna is modelled as current straps in the θ direction at $r = r_s$ with a Faraday screen at $r = r_F$. We chose NSTX-like parameters: $n_c = 5 \times 10^{19}$ m^{-3}, $f = 30$ MHz, $B = 0.32$ T (approximate field at the edge for a 0.55 T on-axis field), $r_c = 0.515$ m, $r_a = 0.575$ m, $r_F = 0.600$ m, $r_s = 0.650$ m, and $r_w = 0.700$ m.

A "mode" refers to global solution which satisfies the wave equation in each region and which is matched at interfaces. Modes assume the form $\tilde{E}_z(r, m, k_\parallel) = \tilde{E}_z(r) \exp(im\theta + ik_\parallel z - i\omega t)$, implying Fourier analysis in the axial and azimuthal directions. With $k_\parallel$ given, $k_\perp$ is fixed in each region by the cold-plasma dispersion, with the slow-wave and vacuum $k_\perp$ always cutoff. Radial profiles are found by the method detailed in Ref. [13]. Each

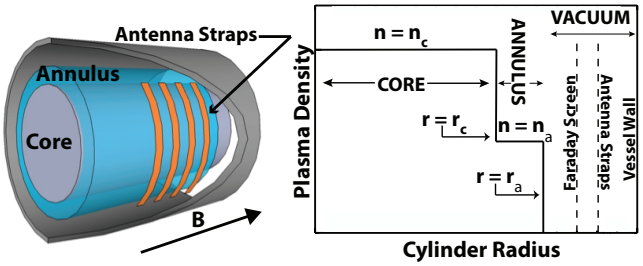

FIG. 1. Model geometry and radial density profile.

region admits four independent solutions. In plasma, there are two fast-wave solutions and two (cutoff) slow-wave solutions; in vacuum there are exponentially decaying and growing E_z (transverse magnetic) and H_z (transverse electric) modes. Four boundary conditions are required at each interface: namely, continuity of E_z, H_z, E_ϕ, and H_ϕ. The twelve total coefficients can be reduced to four by the following: (i) continuity at the core-annulus interface specifies the four annulus coefficients in terms of the core coefficients, (ii) the fields must remain finite at $r = 0$, which requires setting two core coefficients to zero, and (iii) E_z must vanish at the Faraday screen and E_ϕ at the vessel wall, eliminating two vacuum coefficients. We are left with four coefficients α_i, with $i = 1$ the core fast wave, $i = 2$ the core slow mode, $i = 3$ the vacuum E_z mode that vanishes at the Faraday screen, and $i = 4$ the vacuum H_z mode whose E_ϕ component vanishes at the vessel wall. To formulate the final boundary condition, continuity at the annulus-vacuum interface, we form column vectors $(E_z, H_z, E_\phi, H_\phi)$ of the fields required for continuity. Let $\mathbf{v}_i$ be the column vector of form factors that, when multiplied by α_i, give the field components of that solution evaluated at $r = r_a$. For instance, $(E_z^{\rm fast}, H_z^{\rm fast}, E_\phi^{\rm fast}, H_\phi^{\rm fast})_{r=r_a} = \alpha_1 \mathbf{v}_1$. Continuity at $r = r_a$ is then expressed as

$$\alpha_1 \mathbf{v}_1 + \alpha_2 \mathbf{v}_2 = \alpha_3 \mathbf{v}_3 + \alpha_4 \mathbf{v}_4 + \mathbf{So}, \qquad (1)$$

where $\mathbf{So}$ is an inhomogenous source term introduced by the antenna current whose exact form does not concern us here. In the absence of any antenna current ($\mathbf{So} = 0$), modes only exist when $\det(\mathbf{v}_1, \mathbf{v}_2, \mathbf{v}_3, \mathbf{v}_4) = 0$. Define the system dispersion function $F(k_\parallel) = \det(\mathbf{v}_1, \mathbf{v}_2, \mathbf{v}_3, \mathbf{v}_4)$ so that modes exist at the roots of $F(k_\parallel)$.

With an antenna current ($\mathbf{So} \neq 0$), the coefficients α_i are given by Cramer's rule, e.g.,

$$\alpha_4 = \frac{\det(\mathbf{v}_1, \mathbf{v}_2, \mathbf{v}_3, \mathbf{So})}{\det(\mathbf{v}_1, \mathbf{v}_2, \mathbf{v}_3, \mathbf{v}_4)}, \qquad (2)$$

and thus have simple poles at the $k_\parallel$ values of the modes. Therefore, upon inverse Fourier transform to find the total field,

$$E_\theta = \sum_m \int \tilde{E}_\theta(r, m, k_\parallel) J_{\rm ant}(m, k_\parallel) e^{im\theta + ik_\parallel z} dk_\parallel, \qquad (3)$$

the integral reduces to a sum of residues, one for each mode. In Eq. (3), $J_{\rm ant}(m, k_\parallel)$ is the antenna spectral current density and $\tilde{E}_\theta$ the azimuthal electric field per unit antenna spectral current density. The amplitude of each mode is thus given by two factors: (i) the amplitude of $J_{\rm ant}(m, k_\parallel)$ at the $k_\parallel$ of the mode, and (ii) the size of the residue, which is proportional to $(dF(k_\parallel)/dk_\parallel)^{-1}$. We show that the annulus resonance is due to a near vanishing of $dF(k_\parallel)/dk_\parallel$.

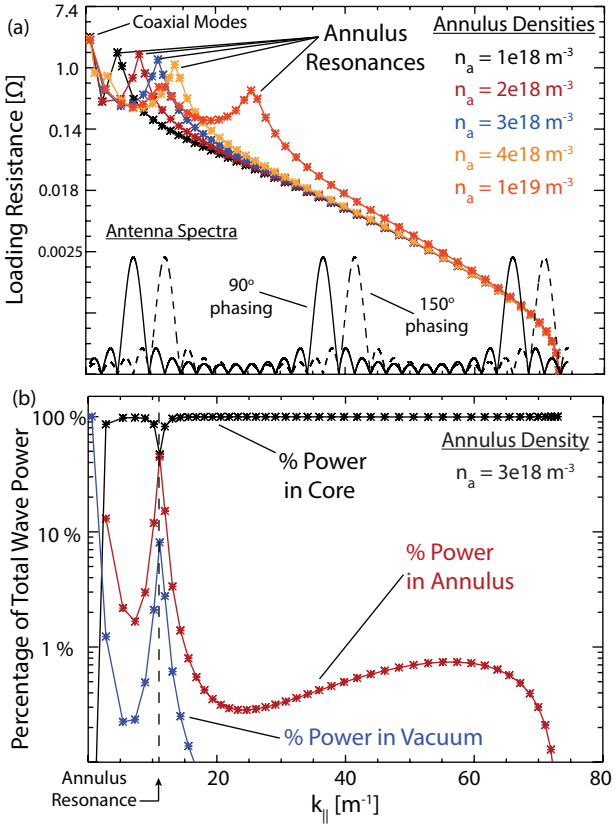

FIG. 2. (a) Loading resistance of $m = 2$ modes for various annulus densities n_a. Antenna spectra for model twelve-strap antenna with 21 cm inter-strap spacing and 90° and 150° phasing are plotted for reference. (b) Percentage of wave power conducted by each mode in the core (black), annulus (red), and vacuum (blue) regions for the $n_a = 3 \times 10^{18}$ m^{-3} case of (a).

The annulus resonances have enhanced amplitudes compared to other modes and carry significant power in the annulus region. Mode amplitude is measured by the total wave power P, calculated by integrating the axial Poynting flux over the cylinder cross-section. We express this as a loading resistance R such that $P = (1/2)RI_{\rm ant}^2$, with $I_{\rm ant}$ the antenna current. The annulus resonances are the peaks in loading resistance in Fig. 2.a. The $k_\parallel$ of the peak depends on the annulus density and can be thus move onto or off of an antenna spectral peak, consistent with the experimental observation that the NSTX SOL

losses are strongly dependent on SOL density [4]. Two resonances appear at high enough density such as the $n_a = 1.0 \times 10^{19}$ m^{-3} curve in Fig. 2.a. $m = 2$ was chosen for illustration purposes; Fig. 2.a is similar for other m. To study the loading curve without complications from any particular antenna spectrum, the calculations in Fig. 2 use a single-strap antenna $J_{\rm ant}(z) = I_{\rm ant}\delta(z)$, which gives equal weight to all modes. The large modes at very low $k_\parallel$ are spurious coaxial modes discussed below. Figure 2.b plots the partition of wave power among the different regions; the axial Poynting flux is integrated over the core, annulus, and vacuum cross-sections. Whereas most modes conduct nearly 100% of their wave power in the core, the annulus resonance conducts 47% in the core, 45% in the annulus, and 8% in the vacuum, while the coaxial mode conducts power entirely in the vacuum region. The term "annulus resonance" is rationalized by the sharp change in radial distribution of Poynting flux shown in this figure.

The very low-$k_\parallel$ modes in Fig. 2.a can be identified as coaxial modes [14, 15], which are distinct from the annulus resonance in several ways. The low-$k_\parallel$ mode resembles the $m = 2$ TEM (transverse electromagnetic) modes found in the coaxial cable formed by replacing the plasma with a conductor. One such mode appears for every m except for $m = 0$, as the $m = 0$ TEM mode has zero E_θ and does not couple to the antenna. Fig. 2.a shows that the $k_\parallel$ of this mode is insenstive to the annulus density, and Fig. 2.b shows that the fields are largely excluded from the plasma and are confined to the vacuum. Despite the enormous loading resistance, this mode is typically considered spurious and removed from analysis [14, 16]. This is because such TEM modes are ordinarily cutoff for $k_\parallel > \omega/c$, but the Faraday screen permits propagation by allowing a current sheet to flow in the axial direction. However, the Faraday screen does not extend to $z = \pm\infty$, so the mode cannot propagate power from the antenna. The annulus resonance is distinct from coaxial modes in several regards. It is not a TEM mode, since it has a substantial H_z component. From Fig. 2.b, the wave fields do penetrate substantially into the core plasma, and the $k_\parallel$ value of the annulus resonance is sensitive to the annulus density. Nor does this mode meet the second criterion of Ref. [14], $k_r \approx 0$, in any region. Finally, coaxial modes do not appear for $m = 0$ but the annulus resonance does.

The annulus resonance appears roughly when a quarter wavelength in the radial direction ($\pi/2k_{\perp,a}^{\rm fast}$) fits into the annulus, although this description is not exact. Figure 3 shows $E_\theta(r)$ for the two annulus resonances seen in the $n_a = 1.0\times10^{19}$ m^{-3} case of Fig. 2.a. While this density is larger than actual densities observed in the NSTX SOL, we use it for illustrative purposes. For the resonance at $k_\parallel = 25.5$ m^{-1}, E_θ undergoes approximately one quarter of a cycle over the annulus (and one half cycle over the annulus plus vacuum regions), while the resonance at $k_\parallel = 11.2$ m^{-1} undergoes approximately three quarters

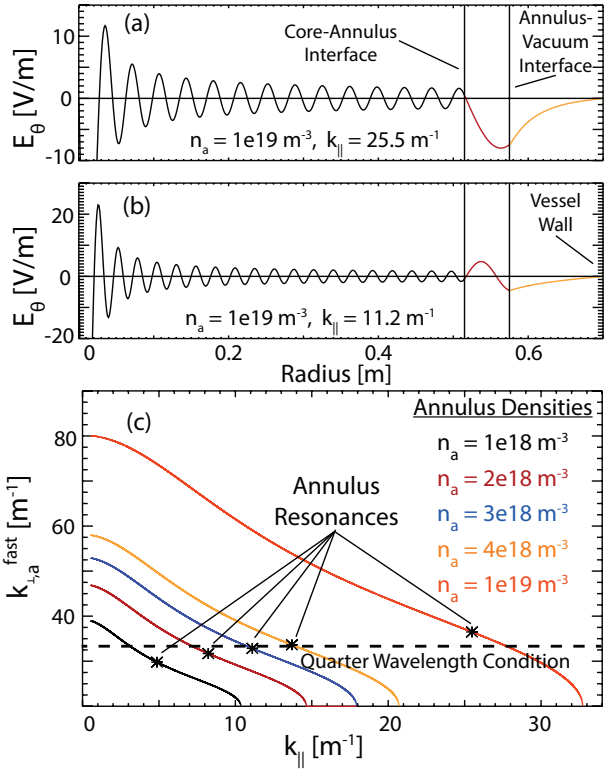

FIG. 3. (a) $E_\theta(r)$ for the annulus resonance at $k_\parallel = 25.5$ m^{-1} for $n_a = 1.0 \times 10^{19}$ m^{-3}. (b) $E_\theta(r)$ for the annulus resonance at $k_\parallel = 11.2$ m^{-1} for $n_a = 1.0 \times 10^{19}$ m^{-3}. (c) $k_\perp^{\rm fast}$ for the different annulus densities in Fig. 2.a, which changes gradually about the quarter wavelength condition.

of a cycle over the annulus and one full cycle over the annulus plus vacuum. Figure 3.c plots $k_{\perp,a}^{\rm fast}$ for each n_a used in Fig. 2.a and indicates the locations of the annulus resonances. While the $k_\parallel$ of the annulus resonance changes strongly with n_a, $k_{\perp,a}^{\rm fast}$ changes only gradually. Changing the core density does not alter the $k_\parallel$-value of the annulus resonance.

The quarter-radial-wavelength condition allows the RF fields from the annulus to match fields in the core in a unique fashion. Typical modes have a particular core fast-wave phase at the core-annulus interface; Fig. 4 plots the core fast-wave fields at $r = r_c$ as a function of $k_\parallel$, and most modes fall primarily at the peaks of H_ϕ and E_ϕ and the nodes of H_z and E_z. The E_θ and H_θ radial profiles typically contain an integral number of half wavelengths plus a quarter. The annulus resonance, however, occurs for a core fast-wave phase 90° out of phase with the other modes and falls at a node for H_ϕ and E_ϕ and a peak for H_z and E_z. It contains an integral number of half wavelengths in the core. The unique fast-wave phase of the annulus resonance at the core-annulus interface explains the high loading resistance of this mode when the core fast-wave fields are propagated to the annulus-vacuum interface. This is done by solving for the four annulus co-

efficients that match a pure core fast wave and evaluating the fields at $r = r_a$; these fields are precisely the components of $\mathbf{v}_1$. Figure 5 shows the annulus resonance falls at maxima in H_ϕ and E_ϕ and very close to the maxima in H_z and E_z at $r = r_a$. Recall that the mode amplitude is inversely proportional to $dF/dk_\parallel$, which is dominated by the term $\det(d\mathbf{v}_1/dk_\parallel, \mathbf{v}_2, \mathbf{v}_3, \mathbf{v}_4)$, because $\mathbf{v}_1$ changes on the scale of the core fast-wave (since the core-slow-wave dependence is cutoff and exponentially growing, $d\mathbf{v}_2/dk_\parallel = \left|k_{\perp,c}^{\rm slow}\right| \mathbf{v}_2$, and $\det(\mathbf{v}_1, d\mathbf{v}_2/dk_\parallel, \mathbf{v}_3, \mathbf{v}_4) \approx 0$ when evaluated at a mode). From Fig. 5, $d\mathbf{v}_1/dk_\parallel$ is small for the annulus resonance because it lies very near a local maximum for all fields, giving a large loading resistance.

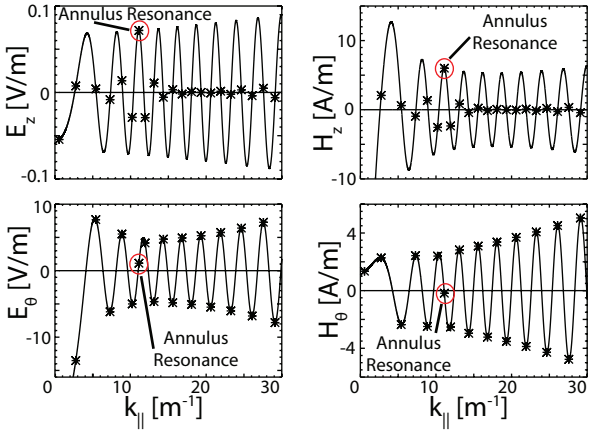

FIG. 4. Core fast-wave fields at $r = r_c$ as a function of $k_\parallel$ with mode locations indicated by stars. $m = 2$ and $n_a = 3.0 \times 10^{18}$ m^{-3}. The annulus resonance is 90° out of phase with other modes.

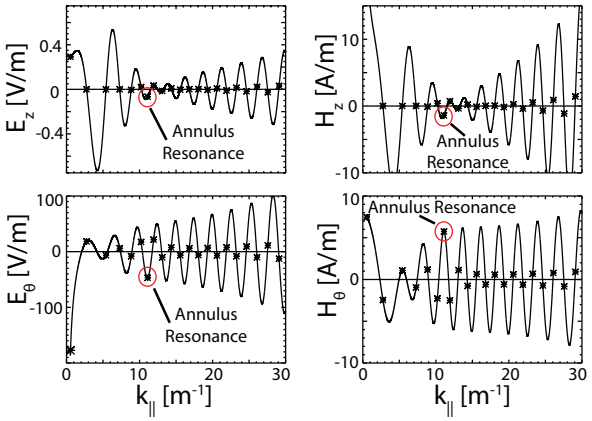

FIG. 5. Similar to Fig. 4 but evaluated at $r = r_a$. The annulus resonance lies near a local maxima for all field components

We propose that the annulus resonances, which appear only when a quarter radial wavelength fits inside the annulus, cause the enhanced RF field amplitude in the SOL of AORSA simulations and the loss of fast-wave power to the divertor of NSTX. This refines the original hypothesis that the losses occur when the density at the antenna exceeds the right-hand cutoff density and would explain why AORSA calculates large RF fields amplitude in the SOL for NSTX and DIII-D for certain SOL densities but not for Alcator C-Mod and EAST even when the antenna density exceeds the cutoff [8]. The annulus resonance occurs when $k_\perp^{\rm fast}(r_a - r_c) \approx \pi/2$, which generalizes to $\int k_\perp^{\rm fast} dr = \pi/2$. Assume $dn_e/dr = n_e/\lambda_n$, with λ_n the SOL density width. There is a critical value, $\lambda_{n,c}$, above which the quarter-wavelength condition is satisfied:

$$\lambda_{n,c} = \frac{\pi/2}{\int_{n_{co}}^{n_{\rm LCFS}} (k_\perp/n_e) dn_e}. \tag{4}$$

We integrate using the cold-plasma dispersion from the cutoff density n_{co} to the density at the last closed flux surface, $n_{\rm LCFS}$. In Table I, $\lambda_{n,c}$ is computed for each case in Ref. [8]. The largest $\lambda_{n,c}$ occur precisely for C-Mod and EAST and greatly exceed those of NSTX and DIII-D; such $\lambda_{n,c}$ is too high to be obtained in a reasonable SOL. For the $n_\phi = 12$ case of NSTX, $\lambda_{n,c}$ is only marginally above the H-mode SOL density width determined in Ref. [17], but, for the $n_\phi = 21$ case, $\lambda_{n,c}$ is significantly larger. This is consistent with experimental observations that (i) the $n_\phi = 21$ phasing has reduced losses, and (ii) the $n_\phi = 12$ heating efficiency can match that of $n_\phi = -21$ for sufficiently low antenna density but can be much reduced otherwise [4]. Finally, scaling the on-axis field from 0.55 T in NSTX to 1.0 T in NSTX-Upgrade increases $\lambda_{n,c}$ for $n_\phi = 12$ to 3.8 cm, meaning that, on NSTX-U, $n_\phi = 12$ phasing, used for current-drive, may enjoy the same low-loss regime as $n_\phi = 21$ phasing on NSTX but with the greater coupling that accompanies lower phasing. The SOL density and density width are highly fluctuating quantities [17, 18]; a detailed study of the phase accrued is needed that accounts not only for the mean profile but for the high-density excursions.

Machine	n_ϕ	f [MHz]	B_T [T]	$n_{e,\rm LCFS}$ [10^{19} m^{-3}]	$\lambda_{n,c}$ [cm]
NSTX	12	30	0.55	0.8	1.8
DIII-D	15	90	1.4	1.0	2.0
DIII-D	15	60	1.4	1.0	3.3
NSTX	21	30	0.55	0.8	3.5
EAST	12	27	1.95	1.0 [19]	7.8
C-Mod	10	80	5.41	1.9	11

TABLE I. $\lambda_{n,c}$ for the cases analyzed in Ref. [8]. $n_\phi = k_\parallel/R$ is the toroidal mode number with R the major radius.

This work was supported by DOE Contract No. DE-AC02-09CH11466. The digital data for this paper can be found in http://arks.princeton.edu/ark:/88435/dsp018p58pg29j. We gratefully acknowledge R. I. Pinsker and S. J.

Zweben for useful discussions and S. M. Kaye and P. T. Bonoli for critically reading the manuscript.

[1] D. Shklyar and H. Matsumoto, "Oblique whistler-mode waves in the inhomogeneous magnetospheric plasma: Resonant interactions with energetic charged particles," *Surveys in Geophysics*, vol. 30, no. 2, pp. 55–104, 2009.

[2] T. Van Doorsselaere, C. S. Brady, E. Verwichte, and V. M. Nakariakov, "Seismological demonstration of perpendicular density structuring in the solar corona," *A&A*, vol. 491, pp. L9–L12, Nov. 2008.

[3] I. Nagano, S. Yagitani, M. Ozaki, Y. Nakamura, and K. Miyamura, "Estimation of lightning location from single station observations of sferics," *Electron. Comm. Jpn. Pt. I*, no. 90, pp. 25–34, 2007.

[4] J. Hosea, R. E. Bell, B. P. LeBlanc, C. K. Phillips, G. Taylor, E. Valeo, J. R. Wilson, E. F. Jaeger, P. M. Ryan, J. Wilgen, H. Yuh, F. Levinton, S. Sabbagh, K. Tritz, J. Parker, P. T. Bonoli, R. Harvey, and N. Team, "High harmonic fast wave heating efficiency enhancement and current drive at longer wavelength on the National Spherical Torus Experimental," *Phys. Plasmas*, vol. 15, no. 5, 2008.

[5] E. F. Jaeger, L. A. Berry, E. F. DAzevedo, R. F. Barrett, S. D. Ahern, D. W. Swain, D. B. Batchelor, R. W. Harvey, J. R. Myra, D. A. DIppolito, C. K. Phillips, E. Valeo, D. N. Smithe, P. T. Bonoli, J. C. Wright, and M. Choi, "Simulation of high-power electromagnetic wave heating in the ITER burning plasma," *Phys. Plasmas*, vol. 15, no. 7, 2008.

[6] D. L. Green, L. A. Berry, G. Chen, P. M. Ryan, J. M. Canik, and E. F. Jaeger, "Predicting high harmonic ion cyclotron heating efficiency in tokamak plasmas," *Phys. Rev. Lett.*, vol. 107, p. 145001, Sep 2011.

[7] N. Bertelli, E. Jaeger, J. Hosea, C. Phillips, L. Berry, S. Gerhardt, D. Green, B. LeBlanc, R. Perkins, P. Ryan, G. Taylor, E. Valeo, and J. Wilson, "Full wave simulations of fast wave heating losses in the scrape-off layer of NSTX and NSTX-U," *Nuclear Fusion*, vol. 54, no. 8, p. 083004, 2014.

[8] N. Bertelli, E. Jaeger, J. Hosea, C. Phillips, L. Berry, P. Bonoli, S. Gerhardt, D. Green, B. LeBlanc, R. Perkins, C. Qin, R. Pinsker, R. Prater, P. Ryan, G. Taylor, E. Valeo, J. Wilson, J. Wright, and X. Zhang, "Full wave simulations of fast wave efficiency and power losses in the scrape-off layer of tokamak plasmas in mid/high harmonic and minority heating regimes," *Nuclear Fusion*, vol. 56, no. 1, p. 016019, 2016.

[9] N. Holtkamp, "An overview of the ITER project," *Fusion Engineering and Design*, vol. 82, no. 514, pp. 427 – 434, 2007. Proceedings of the 24th Symposium on Fusion Technology.

[10] J. C. Hosea and R. M. Sinclair, "Dominant influence of electron inertia on ion cyclotron-wave generation in plasma," *Phys. Rev. Lett.*, vol. 23, pp. 3–7, Jul 1969.

[11] J. C. Hosea and R. M. Sinclair, "Ion cyclotron wave generation in the Model C Stellarator," *Physics of Fluids*, vol. 13, no. 3, pp. 701–711, 1970.

[12] J. C. Hosea and R. M. Sinclair, "Effect of the plasma density profile on ion cyclotron wave generation," *Physics of Fluids*, vol. 16, no. 8, pp. 1268–1272, 1973.

[13] W. P. Allis, S. J. Buchsbaum, and A. Bers, *Waves in anisotropic plasmas*, vol. 1. The MIT Press, 1963.

[14] A. Messiaen, R. Koch, V. Bhatnagar, P. Vandenplas, and R. Weynants, "Analysis of the plasma edge radiation by ICRH antenna," in *Proc. 4th Int. Symp. on Heating in Toroidal Plasmas, Rome*, vol. 1, pp. 315–329, 1984.

[15] R. Pinsker and P. Colestock, "Effect of surface modes on coupling to fast waves in the lower hybrid range of frequencies," *Nuclear Fusion*, vol. 32, no. 10, p. 1789, 1992.

[16] S. Pècoul, S. Heuraux, R. Koch, and G. Leclert, "Numerical modeling of the coupling of an ICRH antenna with a plasma with self-consistent antenna currents," *Computer Physics Communications*, vol. 146, no. 2, pp. 166 – 187, 2002.

[17] S. J. Zweben, R. R. Myra, W. M. Davis, D. A. D'Ippolito, T. K. Gray, S. M. Kaye, B. P. LeBlanc, R. J. Maqueda, D. A. Russell, D. P. Stotler, and the NSTX-U Team, "Blob structure and motion in the edge of NSTX," *Plasma Phys. and Controlled Fusion*, 2016.

[18] J. A. Boedo, J. R. Myra, S. Zweben, R. Maingi, R. J. Maqueda, V. A. Soukhanovskii, J. W. Ahn, J. Canik, N. Crocker, D. A. D'Ippolito, R. Bell, H. Kugel, B. Leblanc, L. A. Roquemore, D. L. Rudakov, and N. Team, "Edge transport studies in the edge and scrape-off layer of the National Spherical Torus Experiment with Langmuir probes," *Physics of Plasmas*, vol. 21, no. 4, p. 042309, 2014.

[19] n_{LCFS} is actually 2.5×10^{18} m^{-3} in the EAST case used in Ref. [8]; this would yield $\lambda_{n,c} = 81$ cm. This large $\lambda_{n,c}$ does supports our hypothesis but mostly because n_{LCFS} is relatively small. For better comparison to the other cases, we use $n_{\mathrm{LCFS}} = 1.0 \times 10^{19}$ m^{-3} in Table 1 to illustrate that $\lambda_{n,c}$ remains high compared to the NSTX and DIII-D cases even when a comparable n_{LCFS} is used.

PPPL PRINCETON PLASMA PHYSICS LABORATORY

Princeton Plasma Physics Laboratory
Office of Reports and Publications

Managed by
Princeton University

under contract with the
U.S. Department of Energy
(DE-AC02-09CH11466)

P.O. Box 451, Princeton, NJ 08543
Phone: 609-243-2245
Fax: 609-243-2751

E-mail: publications@pppl.gov

Website: http://www.pppl.gov